General Disclaimer

One or more of the Following Statements may affect this Document

- This document has been reproduced from the best copy furnished by the organizational source. It is being released in the interest of making available as much information as possible.

- This document may contain data, which exceeds the sheet parameters. It was furnished in this condition by the organizational source and is the best copy available.

- This document may contain tone-on-tone or color graphs, charts and/or pictures, which have been reproduced in black and white.

- This document is paginated as submitted by the original source.

- Portions of this document are not fully legible due to the historical nature of some of the material. However, it is the best reproduction available from the original submission.

DRA

Mechanical Engineering Department
University of Wisconsin--Milwaukee
Milwaukee, Wisconsin 53201

TURBULENT TRANSPORT MODELING OF SHEAR FLOWS AROUND AN AERODYNAMIC WING

Final Report
August 1983

(NASA-CR-166547) NUMERICAL STUDY OF A SEPARATING AND REATTACHING FLOW BY USING REYNOLDS-STRESS TUBULENCE CLOSURE Final Report, 1 Dec. 1982 - 31 Jul. 1983 (Wisconsin Univ.) 30 p HC A03/MF A01 G3/02

N84-17133

Unclas
15042

A Numerical Study of a Separating and Reattaching Flow by Using Reynolds-Stress Turbulence Closure

by

R. S. Amano
Principal Investigator

and

P. Goel
Research Assistant

The report documents research completed during the period of December 1, 1982 through July 31, 1983 under NASA - Ames Research Grant No. NAG 2-160.

TM/83/2

TABLE OF CONTENTS

ABSTRACT

The report addresses itself to a summary of the numerical study of the Reynolds-stress turbulence closure for separating, reattaching, recirculating and redeveloping flow. The calculations were made for two different closure models of pressure - strain correlation. The results were compared with the experimental data. Furthermore, these results were compared with the computations made by using the one-layer and three-layer treatment of k-ε turbulence model which were developed in the first part of this project sponsored by NASA-Ames. Generally the computations by the Reynolds-stress model show better results than those by the k-ε model, in particular, some improvement was noticed in the redeveloping region of the separating and reattaching flow in a pipe with sudden expansion.

NOMENCLATURE

β_1, β_2, β_3	coefficients in the R.S. model of turbulence
C_μ, C_1, C_2, C_s, $C_{\phi 1}$, $C_{\phi 2}$	coefficients in the turbulence model
D	diameter of pipe downstream of expansion
d	diameter of pipe upstream of expansion
H	step height (= (D-d)/2)
k	turbulent kinetic energy (= $\overline{u_i^2}/2$)
Nu	Nusselt number
P_{11}, P_{22}, P_{33}, P_{12}	production rates in RSM
P	turbulence energy generation rate
p	pressure
R_{11}, R_{22}, R_{33}, R_{12}	redistribution terms in RSM
R_{w11}, R_{w22}, R_{w33}, R_{w12}	wall redistribution terms in RSM
Re_D	Reynolds number based on diameter of pipe downstream of expansion
r	radial coordinate
U	mean velocity in x direction
u,v,w	turbulent fluctuating velocity components
V	mean velocity in r direction
x	coordinate parallel to pipe axis
y	nearest distance of the node from the wall
Γ_{eff}	effective diffusivity
ϵ	dissipation rate of turbulence energy
μ	dynamic viscosity
μ_{eff}	effective viscosity (= $\mu + \mu_t$)

μ_t	turbulent dynamic viscosity ($= C_\mu \rho k^2/\varepsilon$)
ν	kinematic viscosity
ρ	density
σ	Prandtl number
σ_k, σ_ε	turbulent Prandtl numbers for diffusion of k and ε
τ	shear stress
ϕ	dependent variable

Subscripts

i,j	tensor notation
t	turbulent values of quantity
w	wall values

1. INTRODUCTION

The heat transfer augumentation which occurs as a result of flow separation and subsequent reattachment is a very important aspect when one is computing the flow over an aerodynamic wing with separation bubbles. While there have been many significant contributions to the flow of this type, current understanding of the process of these flows is still relatively poor partly because the flow mechanism is complex and partly because presently existing turbulence models still have many limitations for a prediction of a wide range of parameters in the separating, reattaching and recirculating flows.

The effect of the recirculating flow was examined by Tani et al. [1] reporting that the maximum back flow velocity is usually over 20% of the free-stream velocity. Bradshaw and Wong [2] and Smyth [3] studied the characteristics of the flow near the reattachment point and found that the turbulence characteristics in the shear layer are usually transported to the downstream of the reattachment.

The above experimental observations suggest that an elliptic approach is always required for reattaching flows. Moreover, it suggests that the large scale-eddies that are developed in the separated free-shear layer persist in the reattachment and redeveloping regions. It was also concluded that the turbulence models which are applicable for mixing-layer flows are also applicable for the reattaching shear flows. In fact, many engineers and researchers have been computing these flows by adopting the standard $k\sim\varepsilon$ model because of its simplicity and success in the prediction of the flow field. However the predictions by the standard $k\sim\varepsilon$ model are not always successful for higher Reynolds number flows or for larger step heights. This

is because the turbulence shear stresses in the separating flow are not computed correctly by using the $k\sim\varepsilon$ model.

Despite the limitations of the $k\sim\varepsilon$ model, the prediction of the turbulence quantities could be improved by employing near-wall models of Chieng and Launder [4] and Amano [5 and 6] in which the local variations of turbulence quantities are evaluated through the viscous sublayer and the overlap layer regions.

A recently simplified version of Reynolds stress turbulence closure was developed and successfully applied for separating and recirculating flows by Hanjalic, Launder and Sindir (shown in Driver and Seegmiller [7]). This model, the so called algebraic-stress model, generally gives better results in the recirculating region, however, the results obtained in the region downstream of the reattachment by using the algebraic-stress model were not as good as the prediction by the standard $k\sim\varepsilon$ model.

In this paper the full Reynolds-stress transport equations are reviewed and adapted for the elliptic flows. For the pressure-strain correlation, two different formulations were applied; one is proposed by Naot et al. [8], and the other by Launder et al. [9]. Because of the complexity of these equations some significant modifications had to be made in the corresponding momentum equations in evaluating diffusive terms by employing the Boussinesq viscosity concept. These modifications are described in the following section. The result of the calculations are presented in the last major section and are compared with the experimental data of the authors' previous work [6]. Comparisons are also made to the computational results by the $k\sim\varepsilon$ model with different near-wall models.

2. MATHEMATICAL FORMULATION

2.1 Equations and Turbulence Models

The governing equations for the models employed in this study can be written in the following general form

$$\frac{1}{r}\left[\frac{\partial}{\partial X}(r\rho U\phi) + \frac{\partial}{\partial r}(r\rho V\phi)\right] = \frac{1}{r}\left[\frac{\partial}{\partial X}\left(r\Gamma_1 \frac{\partial \phi}{\partial X}\right) + \frac{\partial}{\partial r}\left(r\Gamma_2 \frac{\partial \phi}{\partial r}\right)\right] + S_\phi \qquad (1)$$

All the equations solved are summarized in Table 1.

Besides the conventional form of the standard k~ε model, we consider three different turbulence models.

(Model 1) Boussinesq Viscosity Model

This is the ordinary k~ε model, but the Reynolds stresses are computed separately so that this model can be replaced with the Reynolds-stress model (RSM) easily. By using the Boussinesq viscosity concept, all the shear stresses may be expressed as follows:

$$\rho\overline{u^2} = 2/3\ \rho k - 2\mu_t \frac{\partial U}{\partial X},$$

$$\rho\overline{v^2} = 2/3\ \rho k - 2\mu_t \frac{\partial V}{\partial r}, \qquad (2)$$

$$\rho\overline{w^2} = 2/3\ \rho k - \{2\mu_t\ V/r\},$$

$$\rho\overline{uv} = -\ \mu_t\ \left(\frac{\partial U}{\partial r} + \frac{\partial V}{\partial X}\right),$$

The RSM consists of transport equations for four stresses ($\overline{u^2}$, $\overline{v^2}$, $\overline{w^2}$ and $\overline{uv}$) and each term corresponding to the one in Eq. (1) is listed in Table 1. In these equations the productions for these stresses are given as

$$
\begin{aligned}
P_{11} &= -2\rho\left(\overline{u^2}\frac{\partial U}{\partial x} + \overline{uv}\frac{\partial U}{\partial r}\right) \\
P_{22} &= -2\rho\left(\overline{v^2}\frac{\partial V}{\partial r} + \overline{uv}\frac{\partial V}{\partial x}\right) \\
P_{33} &= -\{2\rho\overline{w^2}V/r\} \\
P_{12} &= -\rho\left(\overline{v^2}\frac{\partial U}{\partial r} + \overline{u^2}\frac{\partial V}{\partial x} - \{\overline{uv}\,V/r\}\right).
\end{aligned}
\tag{3}
$$

In this study two different redistribution terms (pressure-strain correlation) are used. One is proposed by Naot et al. [8] and the other by Launder et al. [9].

(Model 2) RSM with redistribution of [8]

$$
\begin{aligned}
R_{11} &= -C_{\phi 1}\rho\varepsilon k^{-1}\left(\overline{u^2} - \tfrac{2}{3}k\right) - C_{\phi 2}\left(P_{11} - \tfrac{2}{3}P\right), \\
R_{22} &= -C_{\phi 1}\rho\varepsilon k^{-1}\left(\overline{v^2} - \tfrac{2}{3}k\right) - C_{\phi 2}\left(P_{22} - \tfrac{2}{3}P\right), \\
R_{33} &= -C_{\phi 1}\rho\varepsilon k^{-1}\left(\overline{w^2} - \tfrac{2}{3}k\right) - C_{\phi 2}\left(P_{33} - \tfrac{2}{3}P\right), \\
R_{12} &= -C_{\phi 1}\rho\varepsilon k^{-1}\overline{uv} - C_{\phi 2}P_{12}.
\end{aligned}
\tag{4}
$$

(Model 3) RSM with redistribution of [9]

$$R_{11} = - C_{\phi 1}\rho\epsilon k^{-1}(\overline{u^2} - \tfrac{2}{3}k) - B_1(P_{11} - \tfrac{2}{3}P)$$

$$- 2B_2\rho k\frac{\partial U}{\partial x} + 2B_3(\rho\overline{u^2}\frac{\partial U}{\partial x} + \rho\overline{uv}\frac{\partial V}{\partial x} + \tfrac{1}{3}P),$$

$$R_{22} = - C_{\phi 1}\rho\epsilon k^{-1}(\overline{v^2} - \tfrac{2}{3}k) - B_1(P_{22} - \tfrac{2}{3}P)$$

$$- 2B_2\rho k\frac{\partial V}{\partial r} + 2B_3(\rho\overline{v^2}\frac{\partial V}{\partial r} + \rho\overline{uv}\frac{\partial U}{\partial r} + \tfrac{1}{3}P), \qquad (5)$$

$$R_{33} = - C_{\phi 1}\rho\epsilon k^{-1}(\overline{w^2} - \tfrac{2}{3}k) - B_1(P_{33} - \tfrac{2}{3}P)$$

$$- \{2B_2\rho kV/r\} + 2B_3(\{\frac{\overline{w^2}V}{r}\} + \tfrac{1}{3}P),$$

$$R_{12} = - C_{\phi 1}\rho\epsilon k^{-1}\overline{uv} - B_1P_{12} - B_2\rho k(\frac{\partial U}{\partial r} + \frac{\partial V}{\partial x})$$

$$+ B_3\rho(\overline{u^2}\frac{\partial U}{\partial r} + \overline{v^2}\frac{\partial V}{\partial x} + \overline{uv}[\frac{\partial U}{\partial x} + \frac{\partial V}{\partial r}]).$$

The generation term P used in Models 1, 2 and 3 is given as

$$P = - \rho(\overline{uv}(\frac{\partial U}{\partial r} + \frac{\partial V}{\partial x}) + \overline{u^2}\frac{\partial U}{\partial x} + \overline{v^2}\frac{\partial U}{\partial r} + \{\overline{w^2}V/r\}). \qquad (6)$$

The constants used in these models are as follows

C_μ	C_1	C_2	C_s	$C_{\phi 1}$	$C_{\phi 2}$	B_1	B_2	B_3
0.09	1.44	1.92	0.25	1.50	0.40	0.764	0.182	0.109

2.2 Low-Reynolds Number Form of RSM

For the incorporation of wall effect into RSM, the wall redistribution term proposed by Launder et al. [9] is used for the low-Reynolds number form of RSM. The terms of low-Reynolds number form are denoted as R_{w11}, R_{w22}, R_{w33}, and R_{w12} for $\overline{u^2}$, $\overline{v^2}$, $\overline{w^2}$, and $\overline{uv}$ respectively (in source term in Table 1). These are expressed as follows for the present flow regions.

$$R_{w11} = \left[0.125\,\frac{\epsilon}{k}\left(\overline{u^2} - \frac{2}{3}k\right) - 0.015\left\{2\overline{uv}\left(\frac{\partial V}{\partial x} - \frac{\partial U}{\partial r}\right)\right\}\right]\frac{\rho k^{3/2}}{\epsilon y}$$

$$R_{w22} = \left[0.125\,\frac{\epsilon}{k}\left(\overline{v^2} - \frac{2}{3}k\right) - 0.015\left\{2\overline{uv}\left(\frac{\partial U}{\partial r} - \frac{\partial V}{\partial x}\right)\right\}\right]\frac{\rho k^{3/2}}{\epsilon y} \qquad (7)$$

$$R_{w33} = 0.125\,\frac{\epsilon}{k}\left(\overline{w^2} - \frac{2}{3}k\right)\frac{\rho k^{3/2}}{\epsilon y}$$

$$R_{w12} = \left[0.125\,\frac{\epsilon}{k}\,\overline{uv} - 0.015\left\{\left(\overline{u^2} - \overline{v^2}\right)\left(\frac{\partial U}{\partial r} - \frac{\partial V}{\partial x}\right)\right\}\right]\frac{\rho k^{3/2}}{\epsilon y}$$

It should be noted here that in the above expression of R_{w11}, R_{w22}, and R_{w12} there is a term -0.015 ( ). In the original paper, this term is positive. The negative sign has been given since the flow geometry here is different from that in the original paper and so the velocity gradients had to be accordingly converted by changing the sign.

For the high-Reynolds number form of RSM, these terms, R_{wij}, are simply set equal to zero.

2.3 Numerical Method

Formulation and discretization of Eq. (1) was performed by using the conventional control volume approach of Patankar [10] by breaking each of the

equations into diffusive, convective and source terms. The systems of equations were made tridiagonal such that they could be solved iteratively by the Tri-Diagonal Matrix Algorithm (T.D.M.A.).

Laminar viscous diffusive terms had to be incorporated in the main governing equations to take into account laminar viscous terms which are significant and adjacent to solid wall boundaries.

The Reynolds stresses were each programmed into individual subroutines. Furthermore, each Reynolds stress has two separate subroutines -- one with the simple equation of Model 1, and the other with the transport equation incorporating both Models 2 and 3.

For the computation of Reynolds stress transport equations, $\overline{u_i u_j}$ is contained in diffusive and source terms of its own $\overline{u_i u_j}$ transport equations. From the numerical point of view a convergence of these transport equations would hardly be attained due to their explicit form. In fact the chance of convergence was minimal when the computation started with an initially guessed $\overline{u_i u_j}$ field. For this reason we adopted a three-pass procedure. Initially the general U and V momentum equations were solved along with the conventional k-ε equation with the generation.

$$P = \nu_t\left[\left(\frac{\partial U}{\partial r} + \frac{\partial V}{\partial x}\right)^2 + 2\left(\frac{\partial U}{\partial x}\right)^2 + 2\left(\frac{\partial V}{\partial r}\right)^2 + 2\left(\frac{V}{r}\right)^2\right] \tag{8}$$

After about 150 iterations, the simple Reynolds stress equations (Model 1) were brought in and the generation term of Eq. (8) was replaced with Eq. (6) to incorporate the Reynolds stresses. After about 20 ~ 50 iterations therefrom, the simple model (Model 1) was replaced by the transport equations of the Reynolds stresses. Complete convergence was achieved after about 100 ~ 150 iterations more.

For the computation of diffusive terms of RSM, these are divided into two groups as

$$D(\phi) = \frac{1}{r}\left[\frac{\partial}{\partial x}\left(r\rho k C_s \overline{u^2}/\varepsilon \frac{\partial \phi}{\partial x}\right) + \frac{\partial}{\partial r}\left(r\rho k C_s \overline{v^2}/\varepsilon \frac{\partial \phi}{\partial r}\right)\right] + D'(\phi) \qquad (9)$$

where

$$\phi = \overline{u^2},\ \overline{v^2},\ \overline{w^2} \text{ or } \overline{uv} \qquad (10)$$

$$D'(\phi) = \frac{1}{r}\left[\frac{\partial}{\partial x}\left(r\rho C_s \overline{uv}/\varepsilon \frac{\partial \phi}{\partial r}\right) + \frac{\partial}{\partial r}\left(\rho k C_s \overline{uv}/\varepsilon \frac{\partial \phi}{\partial x}\right)\right]$$

In Eq. (9) the first term is the diffusive term of Eq. (1) whereas the second term $D'(\phi)$ is taken in as the source term. This modification was done primarily to make programming easier and also to make the equation compatible with the standard form of the transport equation (Eq. (1)).

The cell structure employed in this study is shown in Fig. 1. The scalar quantities such as p, k, and ε are evaluated at grid point P, whereas U and V momentums are computed at staggered grids. For Reynolds stresses, the shear stress $\overline{uv}$ is evaluated at the left-bottom corner of the scalar cell as is done by Pope and Whitelaw [11]. However, normal stresses are computed at different points in the manner indicated in Fig. 1. This arrangement has more advantages in evaluating the terms with shear stress and shear strain combinations than those evaluated at the same scalar node point.

2.4 Boundary Conditions of RSM

Boundary values of the Reynolds stresses at solid wall have been taken from Launder et al. [9], where near the wall

$$\overline{uv} = - U_\tau^2 + \frac{r}{\rho} \left(\frac{dp}{dx}\right)$$

$$\overline{u^2} = 5.1\ U_\tau^2$$

$$\overline{v^2} = 1.0\ U_\tau^2 \qquad (11)$$

$$\overline{w^2} = 2.3\ U_\tau^2$$

and since

$$k \approx 3.5\ U_\tau^2\ , \qquad (12)$$

the boundary values can be expressed in terms of k as follows

$$\overline{uv} = - 0.286\ k + \frac{rdp}{\rho dx}$$

$$\overline{u^2} = 1.457\ k$$

$$\overline{v^2} = 0.286k \qquad (13)$$

$$\overline{w^2} = 0.657\ k$$

So along the solid walls, the above values have been prescribed where at the exit and the symmetry line, zero gradient is assumed as the boundary conditions.

3. PRESENTATION OF RESULTS AND DISCUSSION

As explained earlier, the computational method employed was a three-pass procedure whereas in the conventional k-ε model it was solved up to partial

convergence and then the Reynolds stresses equations were subsequently brought in. Complete convergence for a 32 x 22 grid took about 350 iterations from the start with a total central processor time of about 20 minutes on a UNIVAC 1100 computer. The grid independency tests were also performed for several different non-uniform grid systems and the conclusion was that the present system of 1.03 x 0.95 would provide a compromise between numerical stability and accuracy.

The numerical results of the present computational method are compared to the experimental data of Amano et al. [6]. The Nusselt number or the convective heat transfer coefficient was evaluated by employing the interlinkage between the near-wall variation and the local wall fluxes developed by Jayatilleke and used in Ref. [5].

The results presented and discussed here are for a diameter ratio (d/D) of 0.586 and Reynold numbers (Re_D) of 10,000 and 20,000. Nusselt number distribution along the pipe wall downstream from the expansion as a function of dimensionless axial pipe length is presented and discussed for different models and options of turbulence. Comparison between the computed results of these models and experimental data is also made.

Figure 2 shows the Nusselt number distribution for Reynolds numbers of 10,000, and 20,000. Computational results are obtained using a high Reynolds number form of RSM for both Model 2 and Model 3. The Nusselt numbers computed by Model 3 show generally 4 to 6% lower than those by Model 2. In Fig. 2(a) (Re_D = 10,000), the discrepancy in peak Nusselt number (Nu_{max}) between experimental results and those of Model 3 is about -14% while it is about -8.5% for Model 2. A similar trend is observed in Fig. 2(b) (Re_D = 20,000), the discrepancy in Nu_{max} between experimental results and those of Model 3 being -24% and -22% for Model 2. The Nusselt numbers are, however, more

elevated on account of higher heat trnsfer effects due to increased velocity for Re_D = 20,000.

The general trend compared to the experimental results is similar. The Nusselt number starts out at a low value, begins to increase, reaches a peak value somewhere 5 ~ 8 step heights (x/H) downstream of the expansion and then begins to drop down again to reach a fully developed value.

Although it is difficult to conclude which model predicts Nusselt number better, the results by using Model 3 seem to be lower than those by Model 2 in the redeveloping region which demonstrates that the results by Model 3 are slightly closer to the experimental data.

Figure 3 presents the Nusselt number distribution for Re_D = 10,000 and 20,000 with the low-Reynolds number form by using both Model 2 and Model 3. For Re_D = 10,000, the discrepancy in Nu_{max} for Model 3 is -9% and it is -3% for Model 2. A similar trend can be seen for Re_D = 20,000. The discrepancy in Nu_{max} for Model 3 is -9% and this is -5% for Model 2 (Fig. 3(b)).

In general, although Model 2 predicts a better agreement insofar as Nu_{max} is concerned the overall agreement of Model 3 with the experimental results is better.

Figure 4 shows the Nusselt number distribution for Reynolds number of 10,000 and 20,000 obtained for Model 3 by using both lowand high-Reynolds number forms. It is shown that the levels of Nusselt number are higher by using low-Reynolds number form than the results by high-Reynolds number form. The agreement between computational results and experimental data are generally good in the reattachment region, however, the prediction by low-Reynolds number in the redeveloping region show slightly too high values than that by high-Reynolds number model. It has been demonstrated by Launder et al. [9]

that their low-Reynolds number model predicts well for fully developed channel flows. However, shear strains are not large enough in the reattaching and redeveloping regions. In order to be compatible with the fully developed flow the shear stress - shear strain term (the second term in Eq. (7)) should be sensitized more for the reattaching and redeveloping flows.

Finally, comparisons between the RSM and the k~ε model are shown in Fig. 5 for both Re_D = 10,000 and 20,000. For the computation of k~ε model both the one-layer model and the three-layer model were employed. The one-layer model is the near-wall treatment in which the local variations in viscous effect are not considered at all, whereas the three-layer model is the treatment in which the local variations in viscous sublayer, buffer layer, and fully turbulent region are taken into account [5 and 6]. Figure 5 shows that the RSM gives the best prediction of all, both in reattaching and redeveloping regions.

4. CONCLUSION

From this study the following conclusions can be drawn.

1. The computation of the reattaching and redeveloping flows was improved by incorporating the RMS.
2. The results by Model 2 and Model 3 show about 4-6% difference and particularly in the redeveloping region Model 3 seems to give better results than Model 2.
3. In the reattaching and redeveloping regions the prediction by the low-Reynolds number cannot be improved. It is suggested that the redistribution term of wall effect needs revising for the reattaching and redeveloping flows.

4. Incorporation of RSM improves the prediction more than improvement of $k\sim\varepsilon$ near-wall model. It suggests that one should employ the RSM model rather than refining the $k\sim\varepsilon$ model.

Finally, it could be concluded that, although the RSM improves the prediction in the separating and reattaching flows, the RSM in its present model needs to be modified considerably for the computation of these flows.

REFERENCES

1. I. Tani, M. Iuchi and H. Komoda, Experimental Investigation of Flow Separation Associated with a Step or Groove, Aeronautical Research Institute, University of Tokyo Rep. No. 364, 1961.

2. P. Bradshaw and F.Y.F. Wong, The Reattachment and Relaxation of Turbulent Shear Layers, J. Fluid Mech., Vol. 52, Part 1, pp. 113-135, 1972.

3. R. Smyth, Turbulent Flow over a Plane Symmetric Sudden Expansion, ASME J. Fluids Engng., Vol. 101, No. 3, pp. 348-353, 1979.

4. C. C. Chieng and B. E. Launder, On the Calculation of Turbulent Heat Transport Downstream from an Abrupt Pipe Expansion, Numerical Heat Transfer, Vol. 3, pp. 189-207, 1980.

5. R. S. Amano, On the Calculation of Turbulent Heat and Mass Transport Downstream From an Abrupt Pipe Expansion, AIAA Paper No. 82-1269, 18th Joint Propulsion Conference, 1982.

6. R. S. Amano, M. K. Jensen and P. Goel, Turbulent Heat Transport Downstream From an Abrupt Pipe Expanison, Proc. ASME/JSME Thermal Engineering Joint Conference, Honolulu, 1983.

7. D. M. Driver and H. L. Seegmiller, Features of a Reattaching Turbulent Shear Layer Subject to an Adverse Pressure Gradient, AIAA Paper 82-1029, St. Louis, 1982.

8. D. Naot, A. Shavit and M. Wolfshtein, Interaction Between Components of the Turbulent Velocity Correlation Tensor, Israel J. Tech., Vol. 8, p. 259, 1970.

9. B. E. Launder, G. J. Reece and W. Rodi, Progress in the Development of a Reynolds-Stress Turbulence Closure, J. Fluid Mech., Vol. 68, Part 3, pp. 537-566, 1975.

10. S. V. Patankar, Numerical Heat Transfer and Fluid Flow, McGraw-Hill, 1980.

11. S. B. Pope and J. H. Whitelaw, The Calculation of Near-Wake Flows, J. Fluid Mech., Vol. 73, Part 1, pp. 9-32, 1976.

Table 1 Summary of Equations Solved

Equation	ϕ	Γ_1	Γ_2	S_ϕ
Continuity	1	0	0	0
x-momentum	U	μ_{eff}	μ_{eff}	$-\frac{\partial p}{\partial x} + \frac{\partial}{\partial x}(\mu_{eff}\frac{\partial U}{\partial x}) + \frac{1}{r}\frac{\partial}{\partial r}(r\mu_{eff}\frac{\partial V}{\partial x})$
r-momentum	V	μ_{eff}	μ_{eff}	$-\frac{\partial p}{\partial r} + \frac{\partial}{\partial x}(\mu_{eff}\frac{\partial U}{\partial r}) + \frac{1}{r}\frac{\partial}{\partial r}(r\mu_{eff}\frac{\partial V}{\partial r}) - 2\mu_{eff}V/r^2$
Turbulence energy	k	$\mu + \frac{\mu_t}{\sigma_k}$	$\mu + \frac{\mu_t}{\sigma_k}$	$\rho P - \rho\varepsilon$
Energy dissipation	ε	$\mu + \frac{\mu_t}{\sigma_\varepsilon}$	$\mu + \frac{\mu_t}{\sigma_\varepsilon}$	$C_1\frac{\rho\varepsilon}{k}P - C_2\frac{\rho\varepsilon}{k}^2$
x-normal stress	$\overline{u^2}$	$\mu + \rho k C_s\overline{u^2}/\varepsilon$	$\mu + \rho k C_s\overline{v^2}/\varepsilon$	$P_{11} + R_{11} - \frac{2}{3}\rho\varepsilon + Rw_{11} + D'(\phi)$
r-normal stress	$\overline{v^2}$	$\mu + \rho k C_s\overline{u^2}/\varepsilon$	$\mu + \rho k C_s\overline{v^2}/\varepsilon$	$P_{22} + R_{22} - \frac{2}{3}\rho\varepsilon - \{2\rho\frac{C_s k\overline{w^2}(\overline{v^2} - \overline{w^2})}{\varepsilon\, r^2}\} + Rw_{22} + D'(\phi)$
θ-normal stress	$\overline{w^2}$	$\mu + \rho k C_s\overline{u^2}/\varepsilon$	$\mu + \rho k C_s\overline{v^2}/\varepsilon$	$P_{33} + R_{33} - \frac{2}{3}\rho\varepsilon + \{2\rho\frac{C_s k\overline{w^2}(\overline{v^2} - \overline{w^2})}{\varepsilon\, r^2}\} + Rw_{33} + D'(\phi)$
shear stress	$\overline{uv}$	$\mu + \rho k C_s\overline{u^2}/\varepsilon$	$\mu + \rho k C_s\overline{v^2}/\varepsilon$	$P_{12} + R_{12} - \{\rho\frac{C_s k\overline{w^2}\,\overline{uv}}{\varepsilon\, r^2}\} + Rw_{12} + D'(\phi)$

FIGURE CAPTIONS

FIG. 1 The grid, storage locations and control volumes.

FIG. 2 Nusselt number distribution along the larger pipe wall

a) Re_D = 10,000

b) Re_D = 20,000

FIG. 3 Nusselt number distribution along the larger pipe wall

a) Re_D = 10,000

b) Re_D = 20,000

FIG. 4 Nusselt number distribution along the larger pipe wall

a) Re_D = 10,000

b) Re_D = 20,000

FIG. 5 Nusselt number distribution along the larger pipe wall

a) Re_D = 10,000

b) Re_D = 20,000

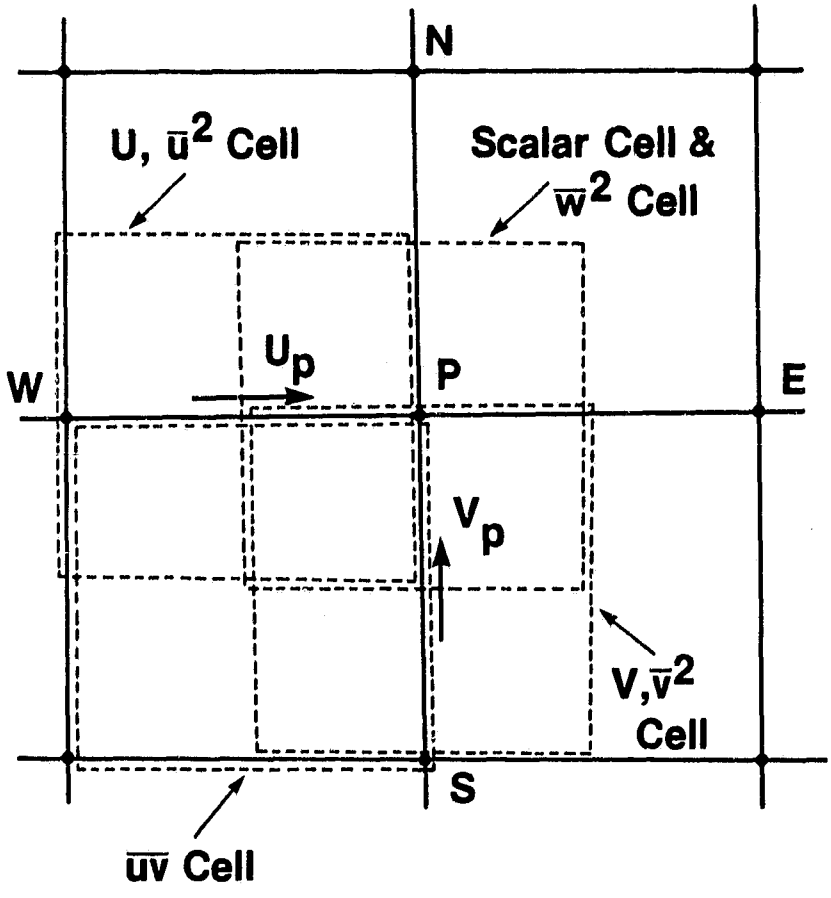

Fig. 1 The grid, storage locations and control volumes. • , grid point, ------, control surface.

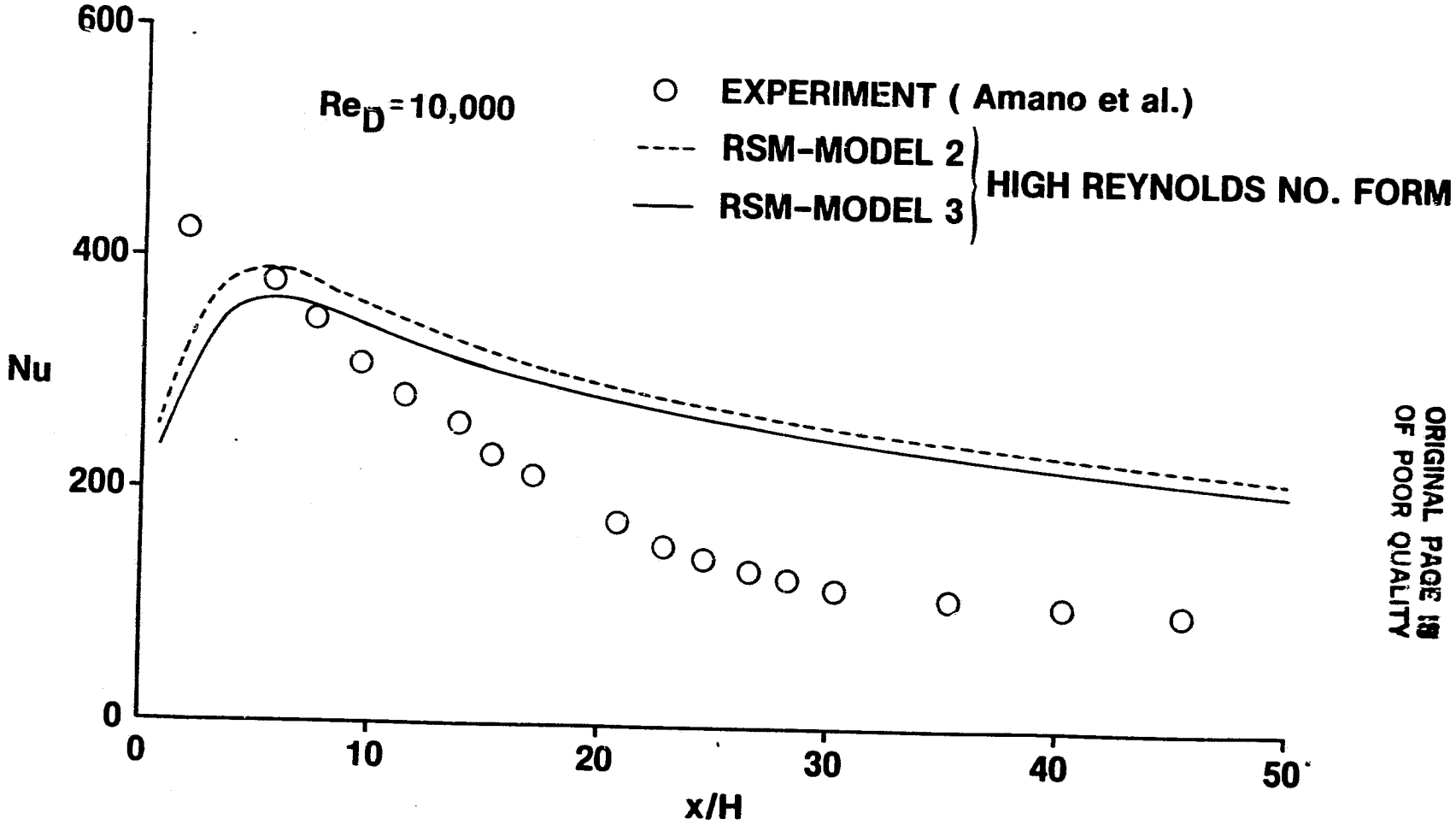

Fig. 2a

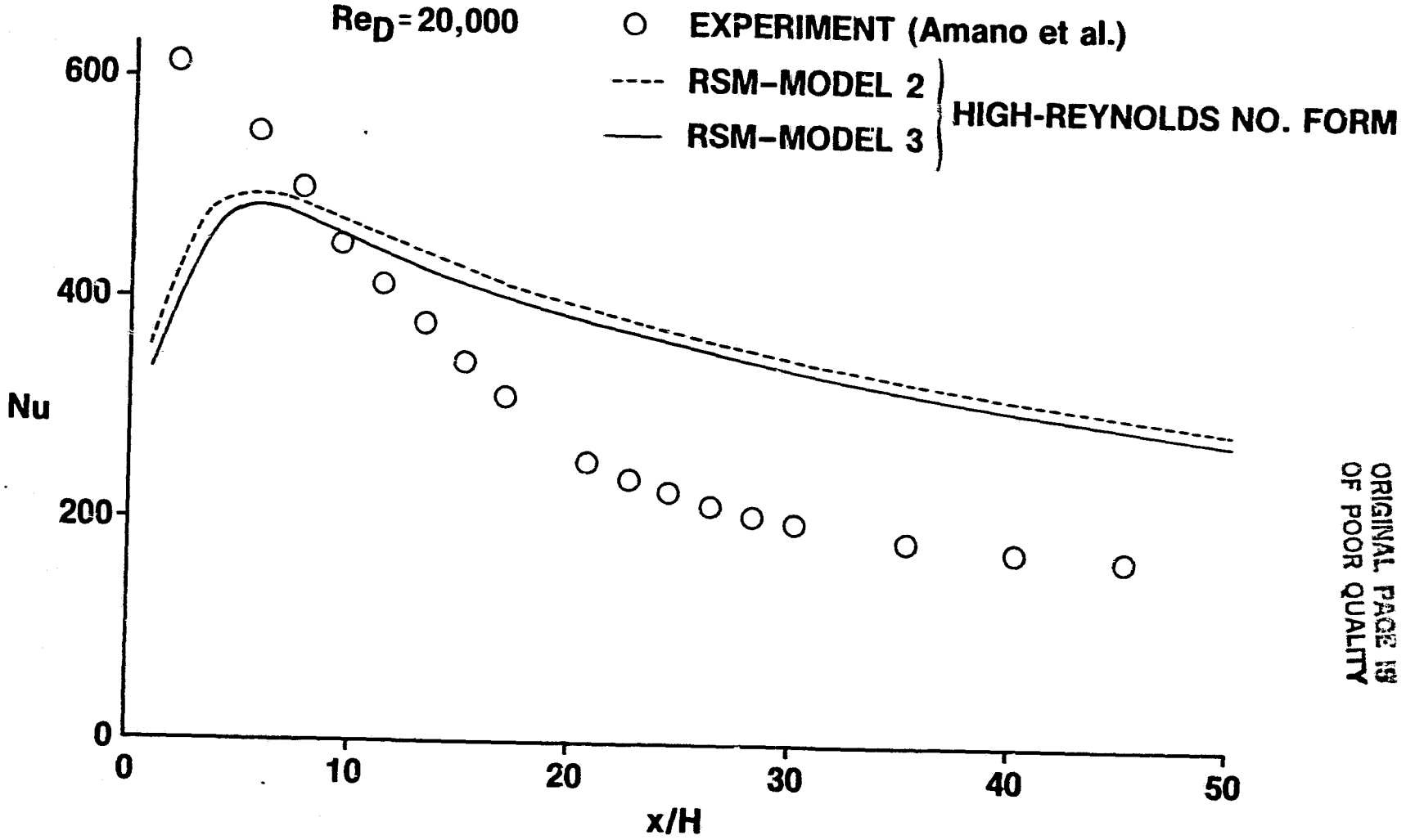

Fig. 2b

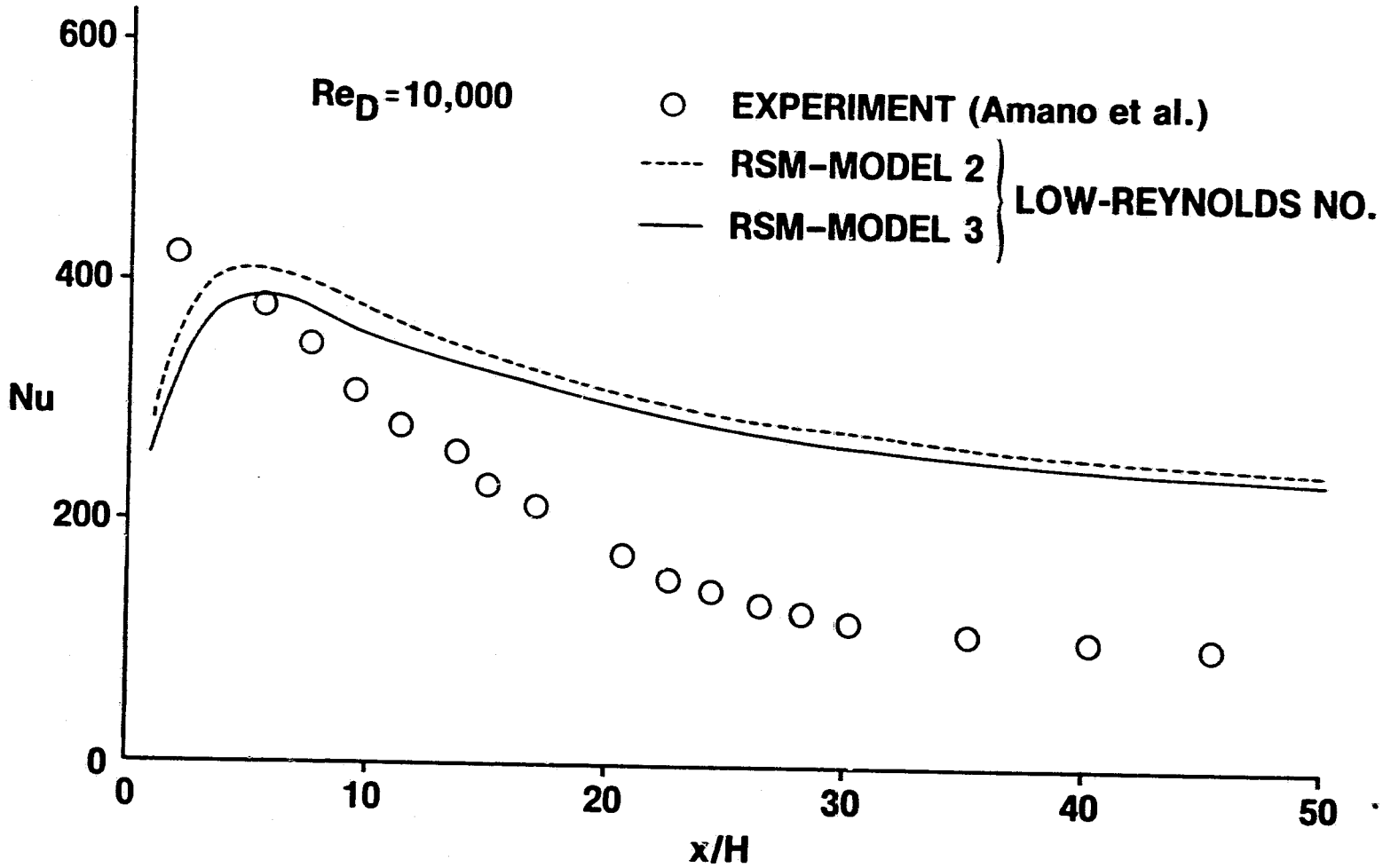

Fig.3a

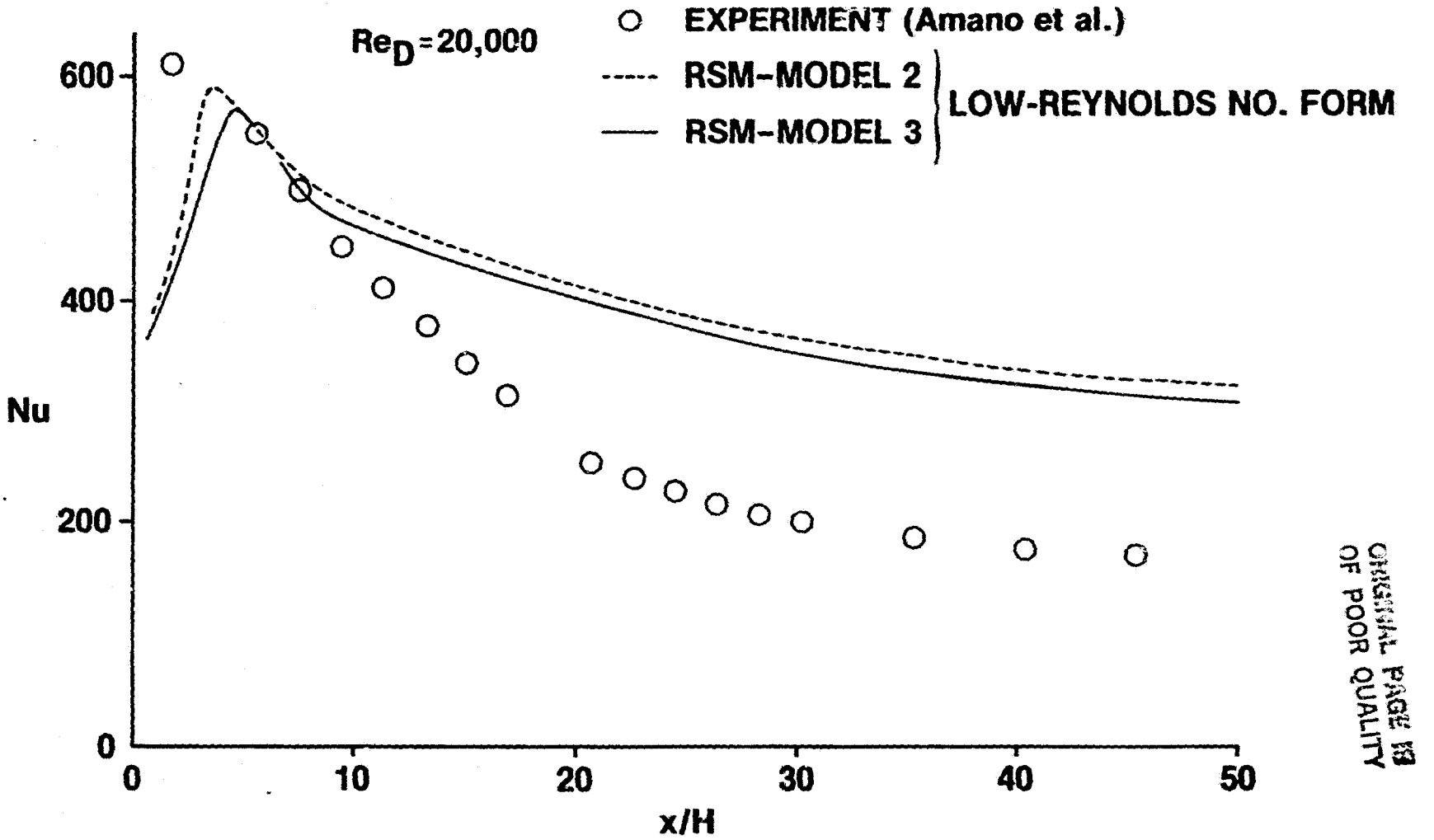

Fig. 3b

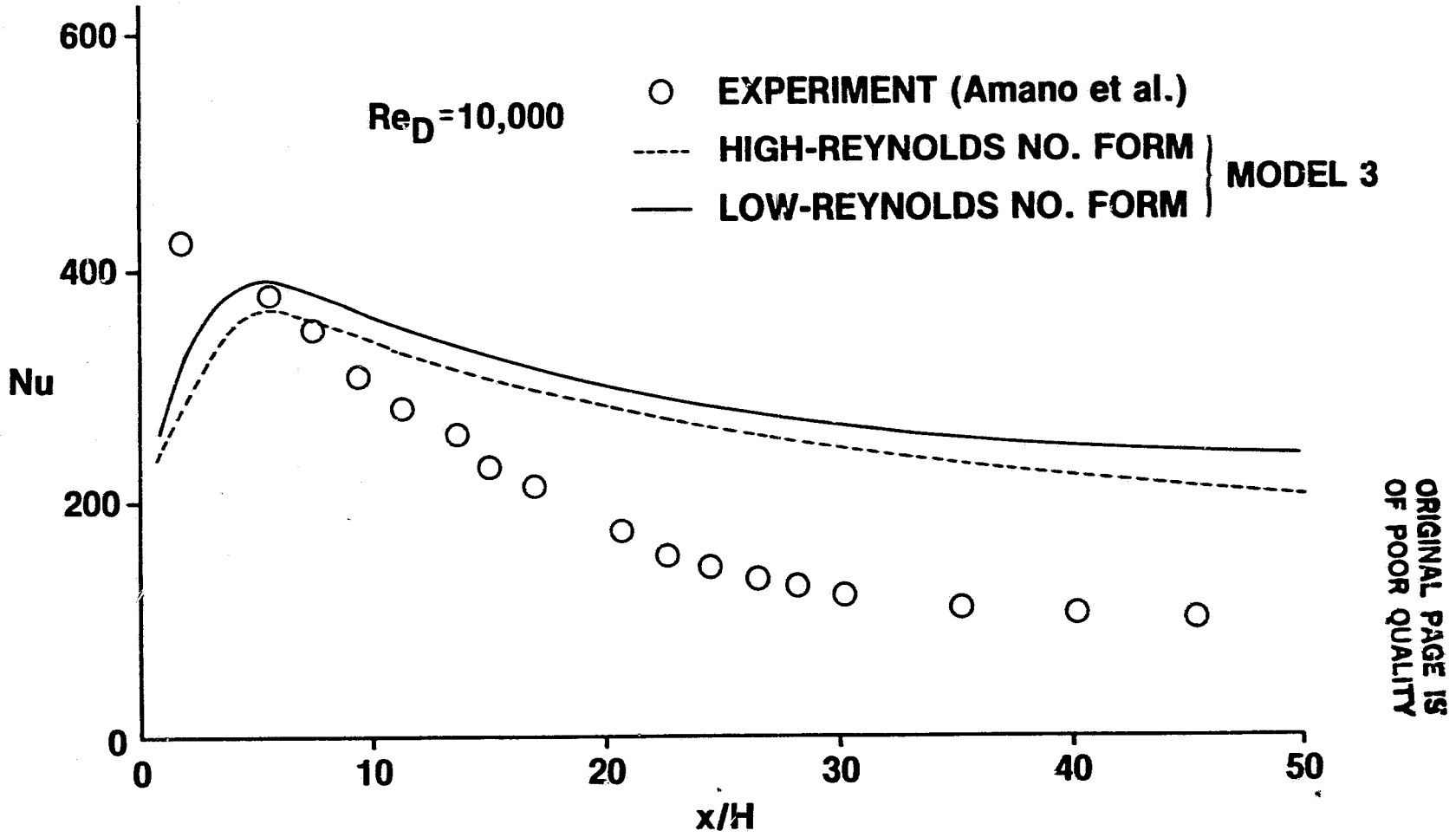
600
400
200
0
Nu
Re_D=10,000
EXPERIMENT (Amano et al.)
HIGH-REYNOLDS NO. FORM
LOW-REYNOLDS NO. FORM
MODEL 3
0
10
20
30
40
50
x/H
ORIGINAL PAGE IS
OF POOR QUALITY

Fig. 4a

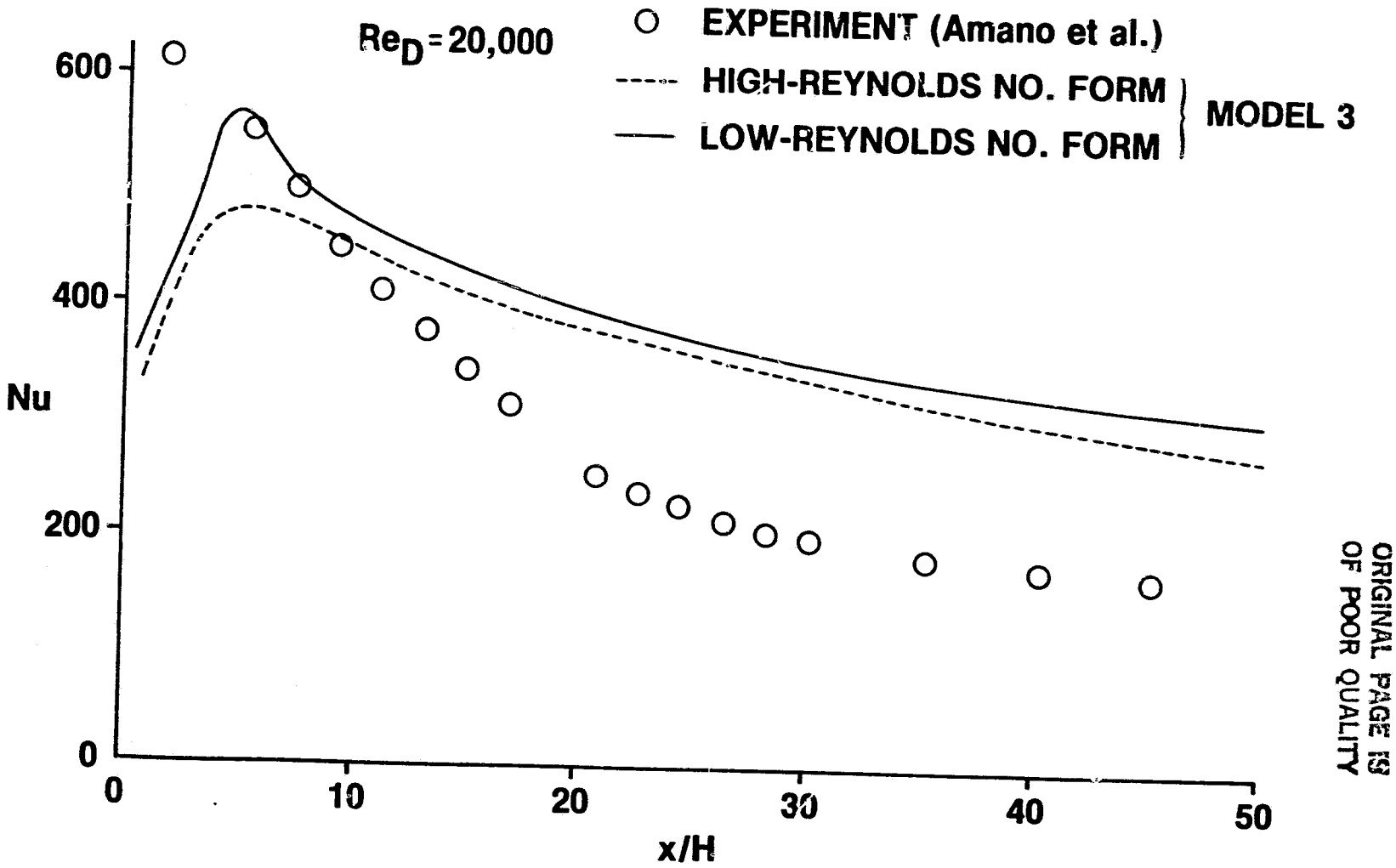

Fig. 4b

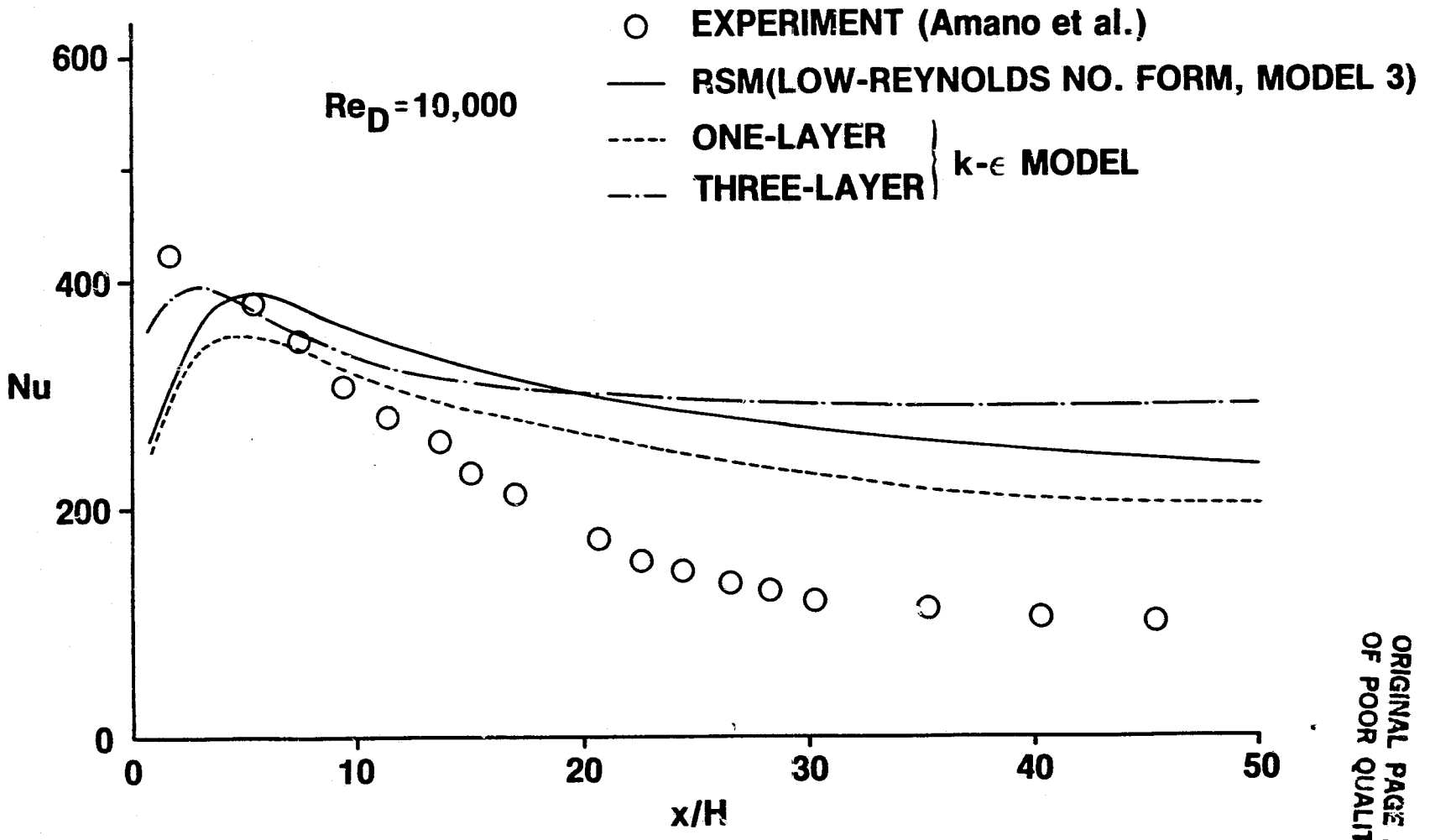

Fig. 5a

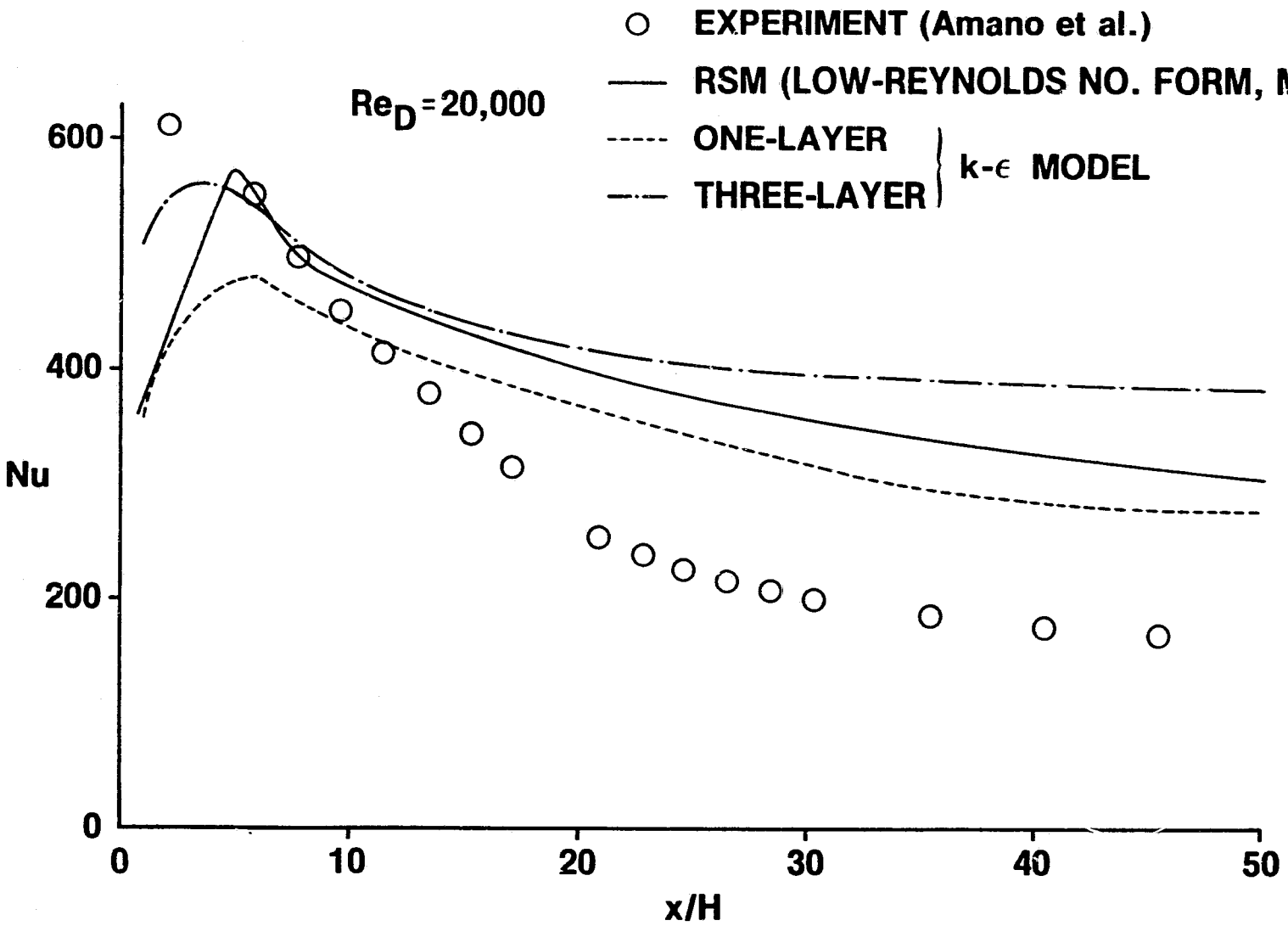

Fig. 5b